Three-dimensional crustal structure of the southern Sierra Nevada from seismic fan profiles and gravity modeling

Moritz M. Fliedner Department of Geophysics, Stanford University, Stanford, California 94305-2215
Stanley Ruppert Lawrence Livermore National Laboratory, Livermore, California 94550
Southern Sierra Nevada Continental Dynamics Working Group*

ABSTRACT

Traveltime data from the 1993 Southern Sierra Nevada Continental Dynamics seismic refraction experiment reveal low crustal velocities in the southern Sierra Nevada and Basin and Range province of California (6.0 to 6.6 km/s), as well as low upper mantle velocities (7.6 to 7.8 km/s). The crust thickens from southeast to northwest along the axis of the Sierra Nevada from 27 km in the Mojave Desert to 43 km near Fresno, California. A crustal welt is present beneath the Sierra Nevada, but the deepest Moho is found under the western slopes, not beneath the highest topography. A density model directly derived from the crustal velocity model but with constant mantle density satisfies the pronounced negative Bouguer anomaly associated with the Sierra Nevada, but shows large discrepancies of >50 mgal in the Great Valley and in the Basin and Range province. Matching the observed gravity with anomalies in the crust alone is not possible with geologically reasonable densities; we require a contribution from the upper mantle, either by lateral density variations or by a thinning of the lithosphere under the Sierra Nevada and the Basin and Range province. Such a model is consistent with the interpretation that the uplift of the present Sierra Nevada is caused and dynamically supported by asthenospheric upwelling or lithospheric thinning under the Basin and Range province and eastern Sierra Nevada.

INTRODUCTION

The deep crustal structure of the Sierra Nevada batholith has been controversial because of contradictory results from seismic studies. Two end-member models have been proposed: a thick Airy-isostatic mountain root (Eaton, 1966), or a thin crust (Carder, 1973) overlying an anomalous mantle that provides isostatic compensation. The time difference between Mesozoic batholith formation (Bateman and Eaton, 1967) and Cenozoic uplift (Huber, 1981) is difficult to reconcile with Airy-root compensation, unless one invokes a mechanism of overcompensation prior to uplift, such as Chase and Wallace's (1988) flexural support by a strong lithosphere that allowed local equilibrium only after breaking by Basin and Range extensional faulting. Alternatively, Crough and Thompson (1977) attributed the forces driving Cenozoic uplift to thermal thinning of the lithosphere that replaced cold, dense subducting oceanic lithosphere with hot, buoyant asthenospheric mantle. The latter model does not require a crustal root to balance the Sierra Nevada and is supported by heat-flow data from the southern Sierra Nevada (Saltus and Lachenbruch, 1991).

Our seismic refraction survey in the Southern Sierra Nevada Continental Dynamics (SSCD) project was designed to resolve the controversy around the crustal structure of the Sierra Nevada (Park et al., 1995; Wernicke et al., 1995). The survey consisted of two crossing lines, with a shot spacing of about 50 km and a maximum shot-receiver offset of 330 km in the north-south line and 390 km in the west-east line (Fig. 1). Nineteen shots were recorded as conventional in-line shots. However, in an effort to address better a three-dimensional problem, four shots were fired in a fan geometry as well: shotpoints (SP) 3 and 4 of the west-east line were reused and recorded in the north-south line and SP 12 and 13 of the north-south line were reused and recorded in the west-east line. Seismic waves from a fan shot (off-line shot) fan across, or sweep out, large parts of the crust in the zone between the receiver line and the shot, thus allowing three-dimensional (3-D) analyses of structure and velocity. A modified west-east line later recorded the NPE (Non-Proliferation Experiment) 1 kiloton explosion at the Nevada Test Site as a fan shot (Fig. 1).

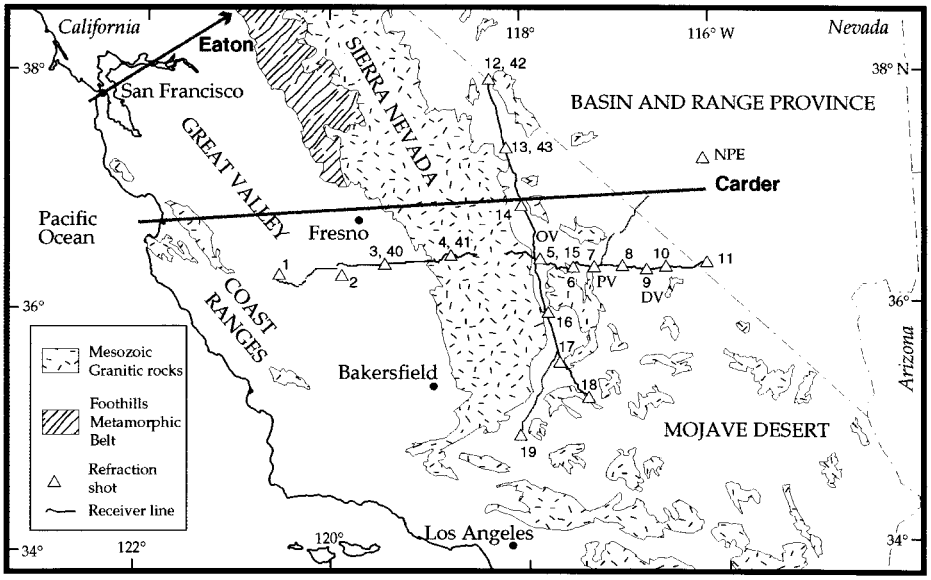

Figure 1. Location of Southern Sierra Nevada Continental Dynamics seismic refraction lines. Shots 1 to 19 were recorded in line. Shots 40 to 43 are fan shots: 40 and 41 recorded in north-south receiver line, 42 and 43 in west-east line. NPE is Non-Proliferation-Experiment shot fired at Nevada Test Site and recorded in west-east line (between SP 1 and 7) and short line from SP 7 toward NPE. OV is Owens Valley, PV is Panamint Valley, and DV is Death Valley. Thick lines locate profiles (Eaton, 1966; Carder, 1973) shown in Figure 2C.

*P. E. Malin (Duke University), S. K. Park (University of California at Riverside), G. Jiracek (San Diego State University), R. A. Phinney (Princeton University), J. B. Saleeby, B. Wernicke, R. Clayton (California Institute of Technology), R. Keller, K. Miller (University of Texas, El Paso), C. Jones (University of Nevada, Reno), J. H. Luetgert, W. D. Mooney, H. Oliver (U.S. Geological Survey), S. L. Klemperer, G. A. Thompson (Stanford University).

Data Repository item 9620 contains additional material related to this article.

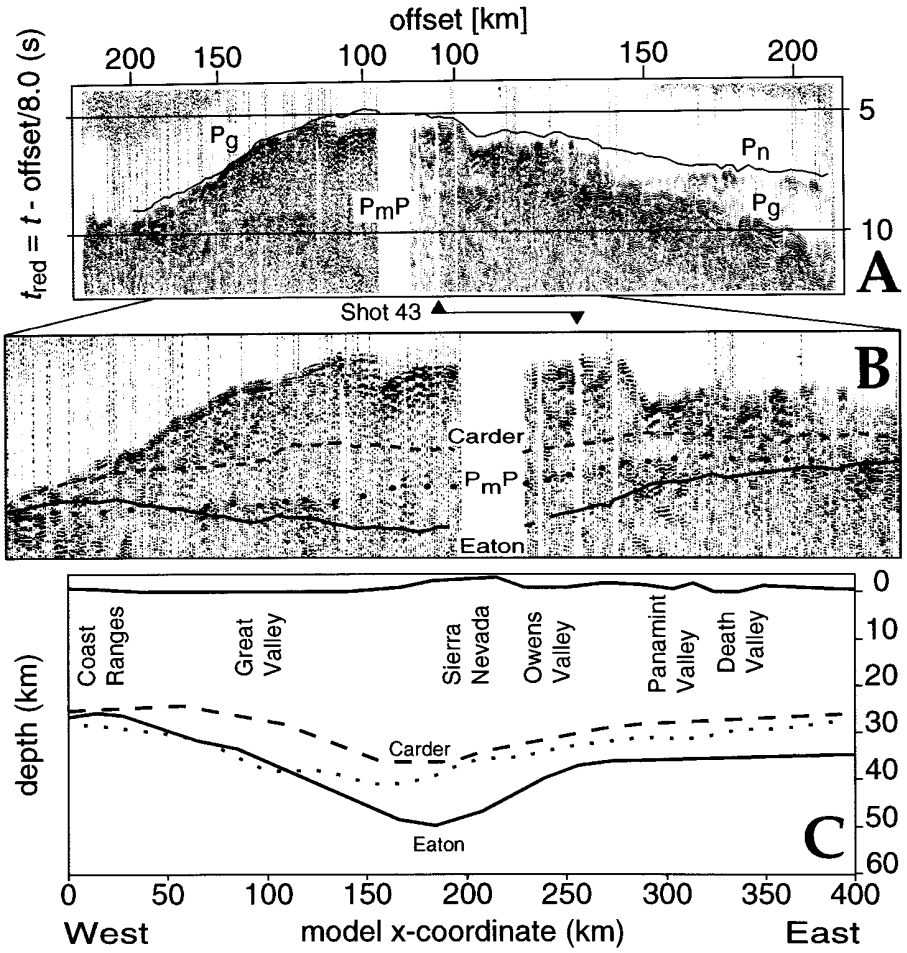

Figure 2. A: Receiver gather of fan shot 43; trace number (west-east coordinate) is plotted against reduced traveltime t_{red}. Shotpoint (triangle) was 95 km north of receiver line. Offset is shot-receiver distance. Traces are amplitude-squared, filtered from 2 to 20 Hz and have 7 s automatic gain control applied. Traces are equally spaced, leading to nonlinear offset scale (abscissa). Solid line is modeled first arrival (predicted times seem to precede observed times, because first arrival is weak or emergent for most of profile and is therefore not visible at this scale; actual root mean square misfit between modeled and observed traveltimes is only 80 ms for this shotpoint). B: Enlargement of A, with picks of P_mP used in this study (dots) compared with calculated traveltimes for two end-member seismic models of Sierra Nevada root: Eaton (deep root, solid line) and Carder (shallow, low-relief Moho, dashed line). C: Cross-sectional cartoon of Carder model (dashed line), Eaton model (solid line), and our final model (dotted line).

SSCD PROFILES—AVAILABLE DATA AND 3-D ANALYSIS

As an example of the fan recordings, the receiver gather from fan shot 43 (Fig. 2A) shows clear crustal (P_g) and mantle (P_n) refractions and Moho reflections (P_mP). (See Appendix 1[1] for more shot gathers.) We compare these data with traveltimes calculated for the actual recording geometry from a priori two-dimensional models extended into the third dimension representing two end-member crustal models of the Sierra Nevada. "Eaton" stands for the Airy-root model following Eaton (1966), and "Carder" for the nearly rootless model following Carder (1973) (Fig. 2C; for location of Eaton and Carder data, see Fig. 1).

Our 3-D interpretation used traveltime data from all the fan and in-line shots, including NPE. The velocities between the lines are less well constrained than directly under the lines because of the small number of fan recordings and the lack of short-offset information that is inherent in the fan geometry (the minimum offsets range from 72 km for SP 41 to 160 km for SP 42; ray coverage in Fig. 3A; data in Appendix 1 [see footnote 1]). Crustal velocities were determined by inverting P_g traveltimes, and although velocities of the lower crust are unconstrained by first arrivals, they are sampled by the secondary part of the P_g phase (beyond the P_n crossover point), albeit more sparsely than the upper crust. Using the crustal velocity model derived from the refracted arrivals, the P_mP reflection times determine the depth to the Moho. P_n arrivals constrain the upper mantle velocities directly beneath the Moho, and they were inverted after we modeled depth to Moho.

The inversion was done using a 3-D finite-difference traveltime modeling and inversion code (modified from Vidale, 1990; Hole, 1992; Hole and Zelt, 1995). Our starting model was one-dimensional, with a linear velocity-depth function. Each step of the iteration consists of traveltime calculation and ray tracing to account properly for position of the rays, and a nonlinear tomographic inversion that updates the velocity model according to the computed traveltime residuals. Because the velocity inversion is nonunique, especially in the off-line regions with sparse ray coverage, we used large smoothing filters on the calculated velocity perturbations in the beginning, and thereafter decreased the filter size gradually. This procedure biases the inversion in favor of large, smooth velocity anomalies; i.e., it should most reliably reveal the first-order features in the velocity structure.

Next, we used our velocities from the P_g inversion for the interpretation of the P_mP reflected arrivals to produce a model that includes a steplike velocity increase from lower crustal to mantle velocities across the Moho, necessary to produce the observed P_mP reflections. P_mP can be recognized clearly on most in-line shots, and then can be transferred to the fan profiles at the line ties to get consistent picks (Appendix 1, see footnote 1). Starting with a constant Moho depth of 30 km, we used a code by Hole and Zelt (1995) to calculate 3-D finite-difference reflection traveltimes and to derive depth perturbations from observed P_mP traveltime residuals. The depth perturbations were gridded to calculate the new Moho; this was iterated until the Moho surface did not change significantly. Finally, P_n arrivals were inverted for mantle velocities after the position of the Moho had been fixed.

Due to uncertainties in picking secondary arrivals consistently and the sparse occurrence of reflection points in three dimensions, the root-mean-square misfit in depth for the final Moho map (Fig. 3B) is 2.2 km. The final model has a root-mean-square misfit of 120 ms (for comparison, in the areas of steepest topography, the elevation difference between *adjacent* receivers corresponds to a relative static shift of about 200 ms); varying the velocities in the constrained parts of the model by more than 0.2 km/s degrades the fit significantly, and we estimate the depth error for our Moho map, including velocity uncertainties, to be ±3 km. (See Appendix 2 [footnote 1] for resolution and error tests for our inversion

[1]Data Repository item 9620, Appendices 1 and 2, is available on request from Documents Secretary, GSA, P.O. Box 9140, Boulder, CO 80301.

Figure 3. A: Map view of first-arrival ray coverage from all shots. Map covers same area as B. B: Contours of Moho depth beneath sea level superimposed on Sierra Nevada batholith. Purple line on east side is crest line. Large dots are reflection points that constrain Moho relief. Red dots are receivers; blue triangles are shotpoints used for interface inversion. Dotted line between shotpoint 1 and X is location of section shown in C. C: Vertical cross section (SP 1 to X in A and B) through velocity model approximately perpendicular to strike of Sierra Nevada. Velocity contour lines (in km/s) and outline of local topography are superimposed on projection of first-arrival ray coverage in 80-km-wide swath centered on section. Interpreted Moho coincides with 7.6 km/s contour.

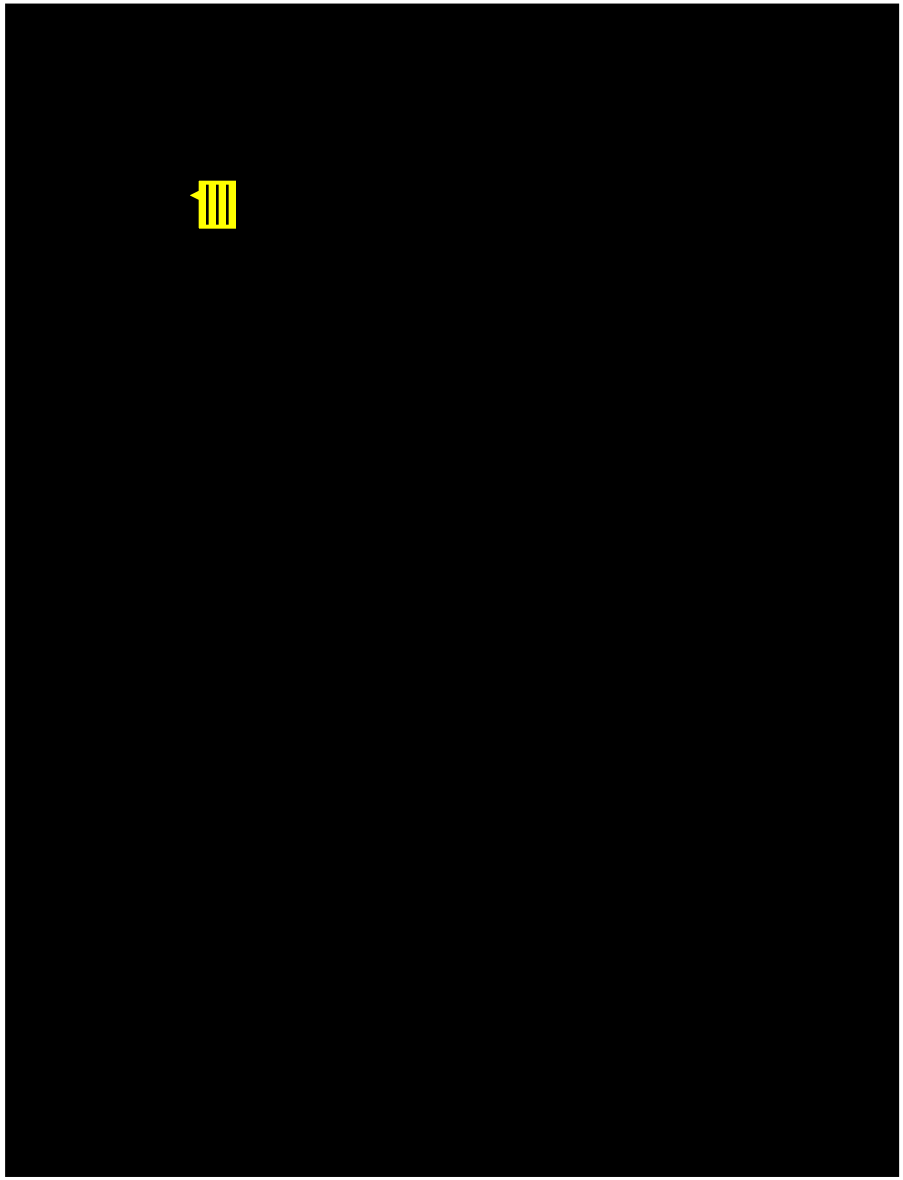

Figure 4. Observed (squares) and modeled (solid line) gravity (Δg) for two-dimensional profile along west-east refraction line. Modeled gravity is referenced to mid-ocean-ridge lithosphere (Lachenbruch and Morgan, 1990). Model topography from Diment and Urban (1981). A: Crustal densities are from velocity-density curve ($V \propto \rho$); mantle density is constant 3280 kg/m^3. B: Crustal densities in Sierra Nevada as in A; density of Great Valley basement is $\geq$2950 kg/m^3, and densities in Basin and Range are $\leq$2750 kg/m^3. C: Crustal densities as in A, but thickness of lithosphere (effective mantle density) varies.

methods, including checkerboard tests for the SSCD aquisition geometry, and further technical details of the modeling.)

RESULTS FROM VELOCITY INVERSION AND MOHO DEPTH MODELING

The most important velocity gradient in our model is the transition from crustal P velocities to P_n velocities of about 7.8 km/s across the Moho. Crustal velocities are lowest in the Sierra Nevada and parts of the Basin and Range province, and high in the Great Valley (Fig. 3C). The Moho (Fig. 3B) deepens northward from around 28 km at the southern end of the Sierra Nevada to 43 km east of Fresno. Figure 3C shows an arbitrary cross section (dotted line in Fig. 3B) through our final 3-D velocity model, chosen as a dip line across the Sierra Nevada through the region of deepest Moho. We mapped a closed contour of 43 km west of shotpoint 14, and the crust thins in the north of our study area. The thickest Sierra Nevada crust is therefore offset 40 km to the west with respect to the crest of the mountain range. Only 20 km east of the highest topography (crestline in Fig. 3B), the crust is as thin as 30–35 km under the north-south line. The thickened crust in the western Sierra Nevada cannot therefore be called a "root" in the sense of local Airy-isostatic compensation. P_mP reflections from the west-east line show Moho depths from 30 to 34 km under the Basin and Range province and 34 to 42 km in the Sierra Nevada; the maximum depth is under the western slopes, and the depth decreases under the Great Valley toward the Coast Ranges to less than 30 km. The crustal thicknesses for the Basin and Range are consistent with other surveys (see Jones, 1987, for a compilation). The Moho depth under the Great Valley is poorly constrained by our data (P_mP arrivals from SP 1 only), but our results are consistent with previous studies (e.g., Holbrook and Mooney, 1987).

IMPLICATIONS FROM COMPARISON WITH GRAVITY

Because the crustal root is offset westward with respect to the High Sierra, it fails to explain the location of the 75 mgal Bouguer gravity trough associated with the Sierra Nevada. Furthermore, the regional gravity difference of 75 mgal between the Basin and Range and the Great Valley (Fig. 4) exists despite similar crustal thicknesses in these regions. The magnitude of the Sierra Nevada gravity low can be roughly modeled using a linear relation between crustal velocities and densities (Oliver, 1977; Thompson and Talwani, 1964; Fig. 4A), and a mantle of constant density (3280 kg/m^3) for a profile along the west-east refraction line (Fig. 4A). We hold the model at the west end at 0 mgal in isostatic equilibrium with the mid-ocean-ridge model described by Lachenbruch and Morgan (1990). This leaves a 50 mgal deficit in modeled gravity for the Great Valley, and a 100 mgal surplus for the Basin and Range. To fit the observed gravity, we consider two extreme possibilities: compensating the residual by crustal anomalies alone (Fig. 4B), or compensating the residual by upper mantle anomalies alone (Fig. 4C). The model shown in Figure 4B achieves a satisfactory fit by assuming the following density anomalies in the Great Valley and Basin and Range crust: 2950 kg/m^3 for the entire basement of the Great Valley (depth range of 5 km to Moho), a density appropriate for the Great Valley ophiolite and mafic basement (Griscom and Jachens, 1990), and a maximum density of 2750 kg m^{-3} for the Basin and Range crust to the east of Owens Valley. The attempt to fit the observed gravity with anomalies in the mantle alone is more difficult, because of the steep gravity gradient between the Great Valley and the Sierra Nevada. In the model shown in Figure 4C, we vary the depth to the asthenosphere by as much as 70 km to achieve the necessary lateral variation in mantle density. Although the anomalous densities in the model in Figure 4B are not unusual for crustal rocks, they deviate considerably from the average crustal density of 2830 kg/m^3 (Christensen and Mooney, 1995) if used for the entire crust. It is furthermore unlikely that the lower crust in the Basin and Range has velocities >6.5 km/s, but densities corresponding to those of felsic rocks. We therefore prefer at least some gravity contribution from an anomalous upper mantle: low velocity, high density under the western Sierra Nevada (possibly eclogite derived from conversion of gabbroic arc crust; Wernicke et al., 1995), or low density under the eastern Sierra and western Basin and Range due to asthenospheric upwelling (Crough and Thompson, 1977).

CONCLUSIONS

The southern Sierra Nevada batholith has a minor crustal thickening with Moho depth no greater than 43 $\pm$ 3 km. This crustal welt is laterally displaced west of the highest topography, and it is insufficient to explain the Sierra Nevada gravity low, which therefore requires laterally varying mantle densities.

ACKNOWLEDGMENTS

The Southern Sierra Continental Dynamics project is supported by the National Science Foundation (NSF) grant EAR-91-19263 to Duke University; this work was supported by NSF grants EAR-92-04998 and EAR-94-05577 to Stanford University and Department of Energy contract W-7405-ENG-48 to Lawrence Livermore National Laboratory. The seismic data were collected with support from the U.S. Geological Survey and the Program for Array Seismic Studies of the Continental Lithosphere (PASSCAL) and are available from the Incorporated Research Institutions for Seismology (IRIS) Data Management Center, via http://www.iris.washington.edu/. We thank Tom Parsons and an anonymous reviewer for helpful reviews.

REFERENCES CITED

Bateman, P. C., and Eaton, J. P., 1967, Sierra Nevada batholith: Science, v. 158, p. 1407–1417.

Carder, D. S., 1973, Trans-California seismic profile, Death Valley to Monterey Bay: Seismological Society of America Bulletin, v. 63, p. 571–586.

Chase, C. G., and Wallace, T. C., 1988, Flexural isostasy and uplift of the Sierra Nevada of California: Journal of Geophysical Research, v. 93, p. 2795–2802.

Christensen, N. I., and Mooney, W. D., 1995, Seismic velocity structure and composition of the continental crust: A global view: Journal of Geophysical Research, v. 100, p. 9761–9788.

Crough, S. T., and Thompson, G. A., 1977, Upper mantle origin of Sierra Nevada uplift: Geology, v. 5, p. 396–399.

Diment, W. H., and Urban, T. C., 1981, Average elevation map of the conterminous United States (Gilluly averaging method): U.S. Geological Survey Geophysical Investigations Map GP-933, scale 1:2 500 000.

Eaton, J. P., 1966, Crustal structure in northern and central California from seismic evidence, *in* Geology of northern California: California Division of Mines and Geology Bulletin, v. 190, p. 419–426.

Griscom, A., and Jachens, R. C., 1990, Tectonic implications of gravity and magnetic models along east-west seismic profiles across the Great Valley near Coalinga, *in* Rymer, M. J., and Ellsworth, W. L., eds., The Coalinga, California, earthquake of May 2, 1983: U.S. Geological Survey Professional Paper 1487, p. 69–78.

Holbrook, W. S., and Mooney, W. D., 1987, The crustal structure of the axis of the Great Valley, California, from seismic refraction measurements: Tectonophysics, v. 140, p. 49–63.

Hole, J. A., 1992, Nonlinear high-resolution three-dimensional seismic travel time tomography: Journal of Geophysical Research, v. 97, p. 6553–6562.

Hole, J. A., and Zelt, B. C., 1995, 3-D finite-difference reflection traveltimes: Geophysical Journal International, v. 121, p. 427–434.

Huber, N. K., 1981, Amount and timing of late Cenozoic uplift and tilt of the central Sierra Nevada, California—Evidence from the upper San Joaquin River basin: U.S. Geological Survey Professional Paper 1197, 28 p.

Jones, C. H., 1987, Is extension in Death Valley accommodated by thinning of the mantle lithosphere beneath the Sierra Nevada, California?: Tectonics, v. 6, p. 449–473.

Lachenbruch, A. H., and Morgan, P., 1990, Continental extension, magmatism and elevation; formal relations and rules of thumb: Tectonophysics, v. 174, p. 39–62.

Oliver, H. W., 1977, Gravity and magnetic investigations of the Sierra Nevada batholith, California: Geological Society of America Bulletin, v. 88, p. 445–461.

Park, S. K., Clayton, R., Ducea, M., Jones, C. H., Ruppert, S., and Wernicke, B., 1995, Project combines seismic and magnetotelluric surveying to address the Sierran root question: Eos (Transactions, American Geophysical Union), v. 76, p. 297–298.

Saltus, R. W., and Lachenbruch, A. H., 1991, Thermal evolution of the Sierra Nevada: Tectonic implications of new heat flow data: Tectonics, v. 10, p. 325–344.

Thompson, G. A., and Talwani, M., 1964, Crustal structure from Pacific basin to central Nevada: Journal of Geophysical Research, v. 69, p. 4813–4837.

Vidale, J. E., 1990, Finite-difference calculation of traveltimes in three dimensions: Geophysics, v. 55, p. 521–526.

Wernicke, B., and 18 others, 1995, Origin of high mountains in the continents: The southern Sierra Nevada: Science, v. 270.

Manuscript received August 21, 1995
Revised manuscript received December 21, 1995
Manuscript accepted December 22, 1995

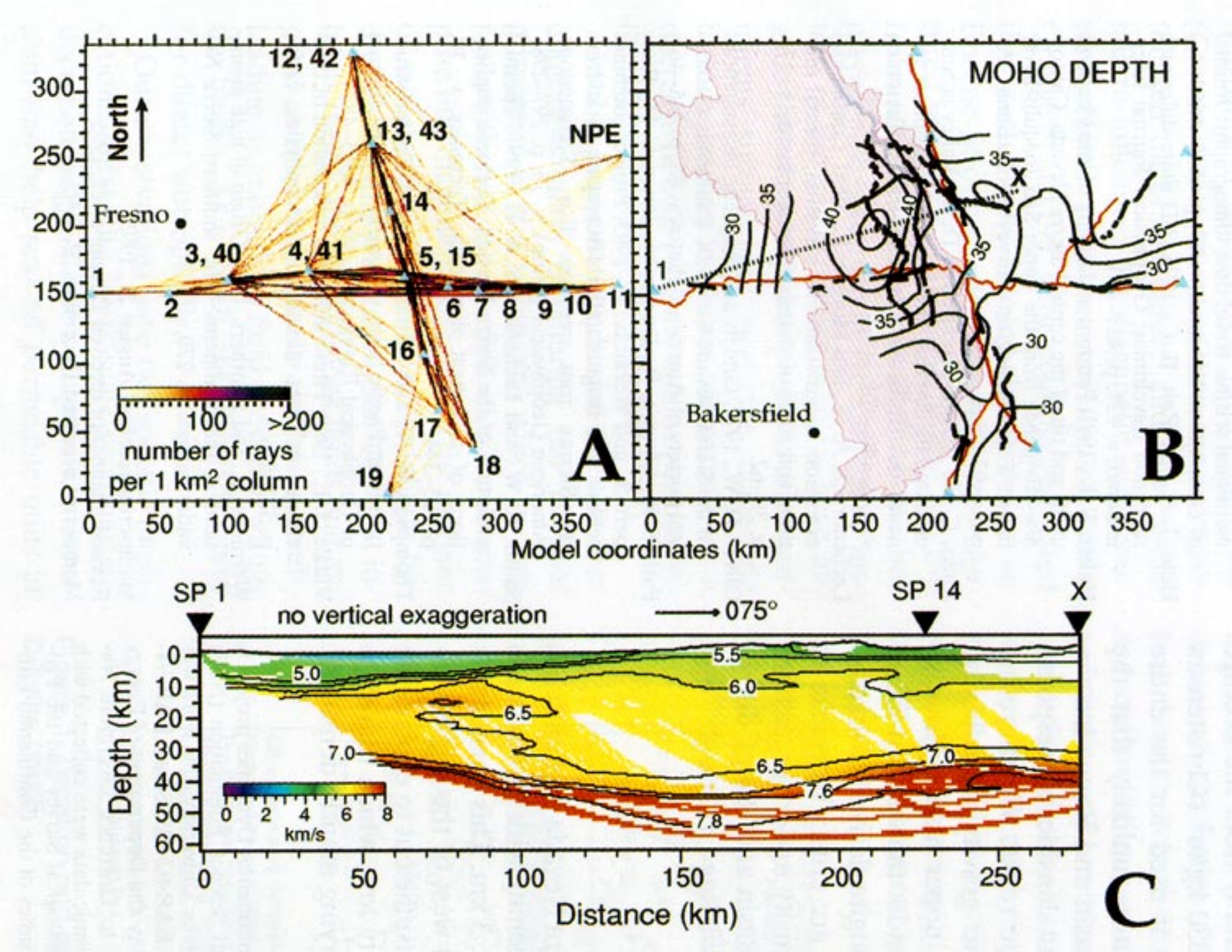
12, 42
13, 43
NPE
North
Fresno
14
3, 40
4, 41
5, 15
1
2
6 7 8 9 10 11
16
17
18
19
0 100 >200
number of rays
per 1 km² column
A
MOHO DEPTH
Bakersfield
B
Model coordinates (km)
SP 1
no vertical exaggeration
075°
SP 14
X
5.0
5.5
6.0
6.5
7.0
7.6
7.8
0 2 4 6 8
km/s
Depth (km)
Distance (km)
C

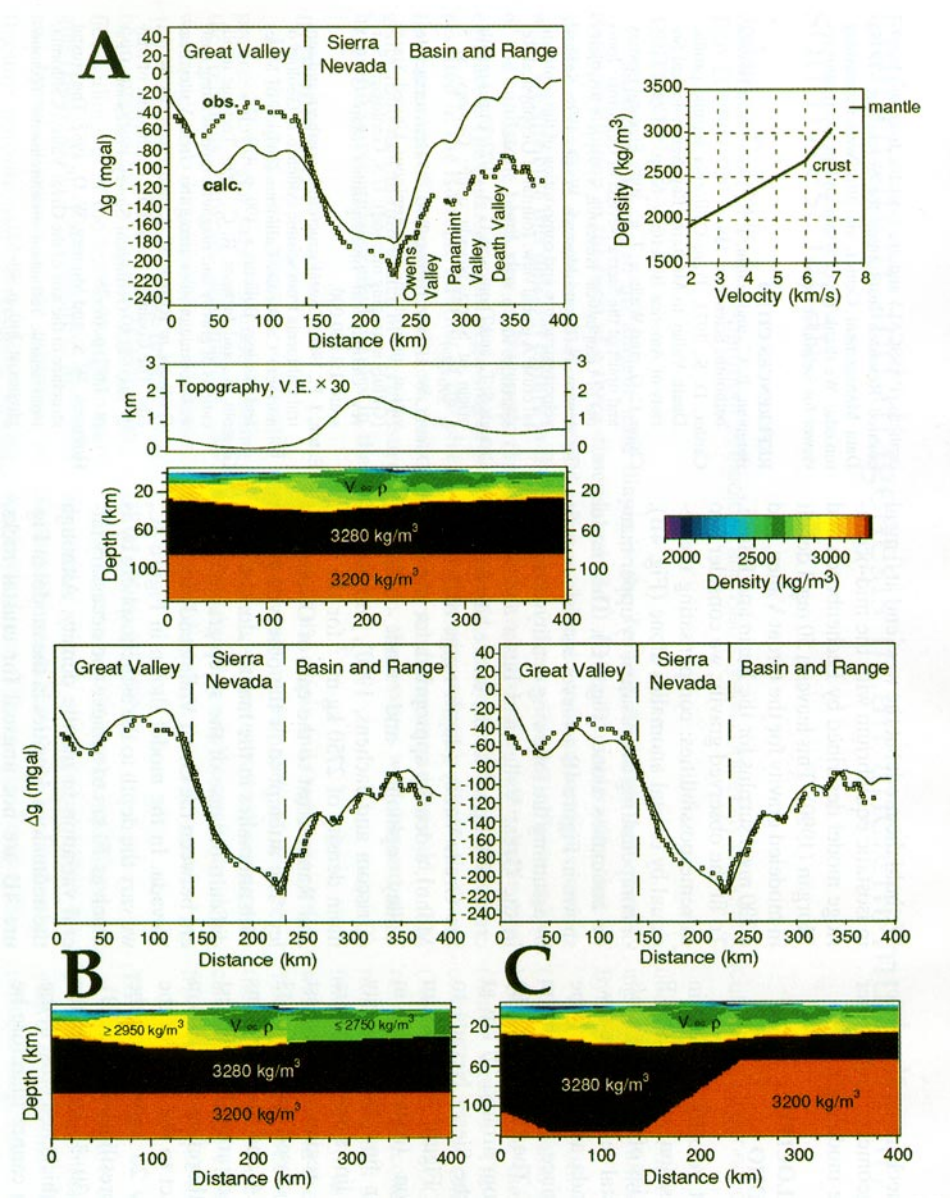
A
Great Valley
Sierra Nevada
Basin and Range
obs.
calc.
Δg (mgal)
Owens Valley
Panamint Valley
Death Valley
Distance (km)
Density (kg/m3)
mantle
crust
Velocity (km/s)
Topography, V.E. × 30
km
Depth (km)
V ∝ ρ
3280 kg/m3
3200 kg/m3
2000 2500 3000
Density (kg/m3)
B
C
≥ 2950 kg/m3
≤ 2750 kg/m3